Nanoscale

Piezoelectricity in WSe_2/MoS_2 Heterostructure Atomic Layers

Journal:	*Nanoscale*
Manuscript ID	NR-ART-05-2018-004394
Article Type:	Paper
Date Submitted by the Author:	30-May-2018
Complete List of Authors:	Yu, Sheng; Hampton University, Hampton, Virginia, USA , Department of Physics Rice, Quinton; Hampton University Tabibi, Bagher; Hampton University, Hampton, Virginia, USA , Department of Physics Li, Qiliang; George Mason University, Electrical and Computer Engineering Department Seo, Felix Jaetae ; Hampton University, Hampton, Virginia, USA , Department of Physics

Piezoelectricity in WSe_2/MoS_2 Heterostructure Atomic Layers

Sheng Yu,[a] Quinton Rice,[a] Bagher Tabibi,[a] Qiliang Li,[b] and Felix Jaetae Seo [a,*]

[a]Advanced Center for Laser Science and Spectroscopy, Department of Physics, Hampton University, Hampton, VA 23668, USA. *jaetae.seo@hamptonu.edu

[b]Department of Electrical and Computer Engineering, George Mason University, Fairfax, VA 22030, USA.

Abstract: Two-dimensional heterostructure of WSe_2/MoS_2 atomic layers has unique piezoelectric characteristics which depends on the number of atomic layer, stacking type, and interlayer interaction size. The van der Waals heterostructure of p- and n-type TMDC atomic layers with different work functions forms a type-II staggered gap alignment. The large band offset of conduction band minimum and valence band maximum between p-type WSe_2 and n-type MoS_2 atomic layers leads to the large electric polarization and piezoelectricity. The output voltages for a MoS_2/WSe_2 partial vertical heterostructure with a size of 3.0 nm × 1.5 nm were 0.137 V and 0.183 V for 4% and 8% tensile strains, respectively. The output voltage of AB-stacking MoS_2/WSe_2 heterostructure was larger than that of AA-stacking heterostructure for 4% tensile strain due to the contribution of intrinsic piezoelectricity and the symmetric condition in out-of-plane. The AB-stacking has a lower formation energy and better structural stability compared to AA-stacking. The large output voltage of nanoscale partial or full vertical heterostructure of 2D WSe_2/MoS_2 atomic layers in addition to the increased output voltage through series connection of multiple nanoscale piezoelectric devices will enable the realization of nano electromechanical systems (NEMS) with TMDC heterostructure atomic layers.

Introduction

Two-dimensional (2D) layered materials of transition metal dichalcogenides (TMDCs) and hexagonal boron nitride (h-BN) are a great interest for the applications of nano electromechanical system (NEMS)[1,2], biomedical devices for monitoring muscle dynamics and arterial repetition rates[3,4], mechanical energy harvesting, and piezoelectronic sensing[5,6]. The 2D TMDCs and h-BN with an odd number layers are asymmetric, while the materials with an even number of layers are centrosymmetric. The piezoelectricity of a single-atomic-layer of h-BN,

MoS_2, $MoSe_2$, or WTe_2 as functions of strain-induced lattice distortion and ionic charge polarization have been studied[7,8] . The orientation of the crystal layer is critical for piezoelectricity[8,9] because the atomic layer exhibits anisotropic angular symmetry of second-order nonlinear polarization in response to applied electric field[5]. It indicates that the symmetry of the atomic layer is broken along the armchair direction, while it is preserved along the zigzag direction[5,10]. An open-circuit voltage of MoS_2 monolayer piezoelectric device with the dimension of 10 μm in length and 5 μm in width was reported to be 18 mV for 0.53% tensile strain[6]. The magnitude of output voltage is critical for the realization of 2D atomic layers for piezoelectric devices.

The 2D TMDC atomic layers have a pool of scientific merits including a weak van der Waals coupling between layers[11], strong covalent in-plane bonds[12], large exciton binding energy[13,14], reduced dielectric screening out-of-plane[15], and potential boson-boson or boson-fermion entanglements[16]. The combination of different atomic layers enables the heterostructure piezoelectric effect. The van der Waals heterostructure of p- and n-type TMDC atomic layers with different work functions forms a type-II staggered gap alignment[17,18]. The large band offset of conduction band minimum (CBM) and valence band maximum (VBM) between p- and n-type atomic layers induces significantly large electric polarization and piezoelectric conversion[19,20]. The stacking styles and conditions of heterostructure with different strain modify the van der Waals (vdW) interaction energy between layers, energy band structure, and optical energy gap[21,22], while the anisotropy of second-order nonlinear polarization along the angle between the incident polarization and the armchair direction of atomic layer identifies the stacking style of heterostructure[23].

Among the TMDCs (MX_2; M=Mo, W; X=S, Se, Te), the experimental results of piezoelectricity in MoS_2 atomic layers were reported early.[6, 24-29] The atomic layers could be prepared by mechanical exfoliation,[6, 24, 25] chemical vapor deposition,[26-28] or liquid phase exfoliation[29] techniques. The piezoelectricity of MoS_2 atomic layer which was prepared by mechanical exfoliation[6] was 15 mV and 20 pA for the 0.53% tensile strain which corresponds to a power density of 2 mW/m^2 and 5.08% mechanical-to-electrical energy conversion efficiency. In this report,[6] the mechanical energy of cyclic stretching and releasing of odd-layer MoS_2 flakes resulted in the oscillating electrical energy. The piezoelectric coefficient in a free-standing single

layer of MoS_2 was experimentally estimated to be $e^{11} = 2.9 \times 10^{-10}$ C/m.[24] The piezoresistivity as a function of strain for MoS2 atomic layers was also reported.[25]

The mechanically exfoliated MoS_2 flakes are not suited to a large scale device fabrication because the size of flakes is in nano scale and the thickness of flakes are not even. A chemical vapor deposition (CVD) technique could prepare triangular monolayer MoS_2 (1L-MoS_2) flakes in the sizes of several micrometers.[26-28] Using an atomic force microscope, the conductive tip-induced current density in MoS_2 piezoelectric device was 65 mA/cm^2, while that of graphene piezoelectric device displayed just a noise current.[26] The conductivity of MoS_2 devices could be actively modulated by the electric field due to the piezoelectric charge polarization under the strain variation.[27] In this report, the polarized charges altered the Schottky barrier height at both contacts. The barrier height increased as the compressive strain was increased, and decreased as the tensile strain was increased. The output power from a nanogenerator in the armchair direction of MoS_2 was around two times higher than that in the zigzag direction for the same strain of 0.48% and strain velocity of 70 mm/s.[28] In this article, the piezoelectric coefficient d_{11} of chemical vapor deposition grown MoS_2 single layer was estimated to be ~3.78 pm/V. However, the scalability of electronic device with MoS_2 with CVD is limited due to the electrode preparation with an electron beam lithography.[29] The MoS_2 flakes with liquid phase exfoliation (LPE) such as solution casting, spray coating, or inkjet printing was introduced for the scalable fabrication of electronic devices.[29] Using the LPE technique, the large piezoelectric current density, 100 mA/cm^2, of MoS_2 single layer was reported.[29] The large piezoelectric current density was ascribed to the edges of stepped multiple layer MoS_2 flakes.[29]

For the atomic layer heterostructure, the spontaneous polarization of phosphorus/MoS_2 and WS_2/MoS_2 was reported[32, 33] however the piezoelectricity of partial and full TMDC atomic layer heterostructure with number of layers, stacking style, and interlayer interaction size are unprecedented. In this article, the piezoelectric properties of MoS_2/WSe_2 heterostructure were characterized. The MoS_2/WSe_2 heterostructure display the largest band offset between CBM and VBM[34] among the combinations of Mo and W transition metal ions and Se and S dichalcognides. The large band offset between CBM and VBM implies the large electronic polarization between p-type and n-type atomic layers. The first principle study of MoS_2/WSe_2 partial vertical heterostructure with a size of 3.0 nm × 1.5 nm showed output voltages of 0.137 V and 0.183 V for 4% and 8% tensile strains, respectively. The large output voltage within only a few

nanometer scale of heterostructure atomic layers is attributable to the large electric polarization. In addition, a series connection of nanoscale piezoelectric device will significantly increase the output voltage for the realization of NEMS with TMDC heterostructure. A schematic drawing of a portable and wearable piezoelectric adhesive bandage (or bracelet around the wrist) of WSe_2/MoS_2 partial stacked heterostructure on the wrist in large scale is shown in figure 1 for monitoring muscle dynamics and arterial repetition regulation.

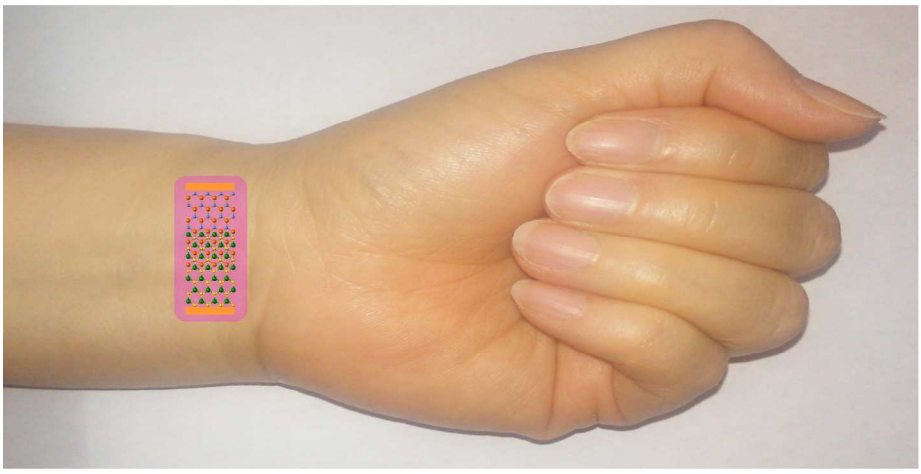

Figure 1. Schematic drawing of a portable and wearable piezoelectric bandage of WSe_2/MoS_2 partial stacking heterostructure on the wrist in large scale.

Methodology

The piezoelectronic properties of 2D WSe_2/MoS_2 heterostructure was investigated by the first principle calculations with density functional theory (DFT) in Virtual Nanolab ATK package[35]. The Localized Density Approximation (LDA) exchange correlation with a double zeta polarized (DZP) basis was used with a mesh cut-off energy of 150 Ry[36]. 1× 1× 50 Monkhorst-Pack k-grid mesh was employed with more k-points in transport direction[37]. All atomic positions and lattice constants were optimized by using the Generalized Gradient Approximations (GGA)[38] with the maximum Hellmann-Feynman forces of 0.05 eV/Å[39]. Pulay-mixer algorithm was employed as iteration control parameter with a strict tolerance value[40] of 10^{-5}. The self-consistent field (SCF) calculations were used to guarantee full convergence within the iteration steps. The maximum number of fully SCF iteration steps[36] was set to 1000. The dirichlet boundary condition was used along the transport direction[41], and the periodic boundary condition was utilized along other two vertical directions[42]. The electronic temperature was set to 300 K for all the simulations.

The first principle calculation includes the piezoelectricity of partial and full vertical WSe_2/MoS_2heterostructure for different number of atomic layer, stacking type, and interlayer interaction size.

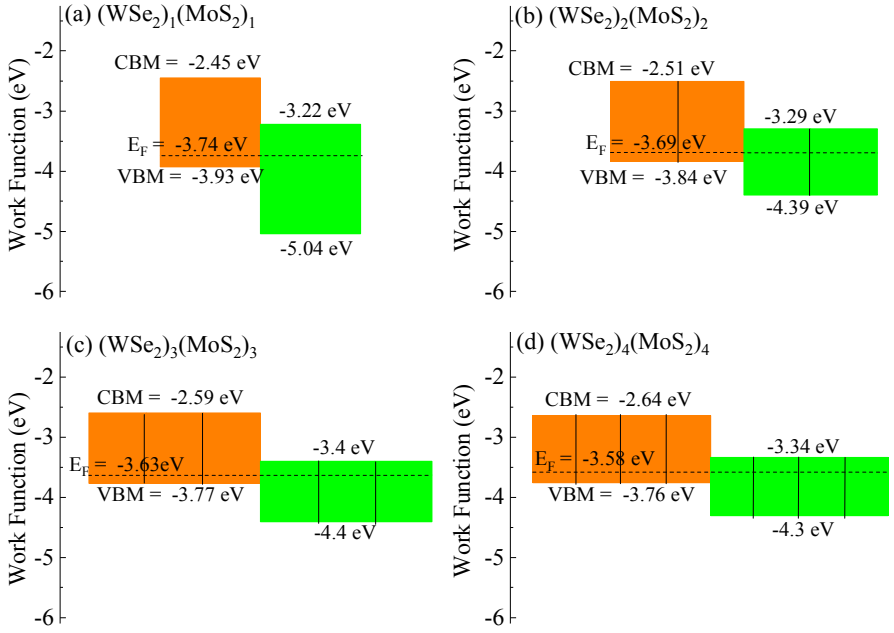

Figure 2. Energy band diagram of $(WSe_2)_m/(MoS_2)_m$ heterostructure for (a) 1 layer; (b) 2 layers; (c) 3 layers and (d) 4 layers. The Fermi energy level is indicated by E_F. The forbidden band is marked by the colored region. The conduction band minimum (CBM) and valence band maximum (VBM) are numerated.

Results and Discussion

Among all the possible combinations of TMDCs materials composing 2D heterostructure, as shown in Supplementary Information (figure 1s), the band gap of MoS_2/WSe_2 is lowest for various structure thickness of 1-4 layers. The narrowing of the electronic band gap E_g would lead to the larger piezoelectricresponse. Therefore, $(WSe_2)_m/(MoS_2)_m$ was slected for investigating the piezoelectricity of atomic layer heterostructure. The energy band diagrams of $(WSe_2)_m/(MoS_2)_m$ heterostructure with m-layers of p-type and n-type atomic layers are shown in figure 2. The larger band offset would have a stronger polarization response in the heterostructure. WSe_2 and MoS_2 atomic layers act as p-type and n-type materials. The heterostructure of p- and n-type TMDC atomic layers with different work functions formed a type-II staggered gap alignment. The Fermi level (E_F) is located near the VBM of WSe_2 and CBM of MoS_2. This indicates that the high density free holes accrue at WSe_2 atomic layer, and the high density free electrons build

up at MoS_2 atomic layer. Then, the electric polarization between p-type WSe_2 and n-type MoS_2 atomic layers is induced in the WSe_2/MoS_2 heterostructure. The interlayer energy difference between WSe_2 and MoS_2 is tunable from 0.71 eV to 0.42 eV as the number of layers is changed from 1 to 4. The larger band offset would have the larger piezoelectronic response in the heterostructure.

I. Partial vertical heterostructure

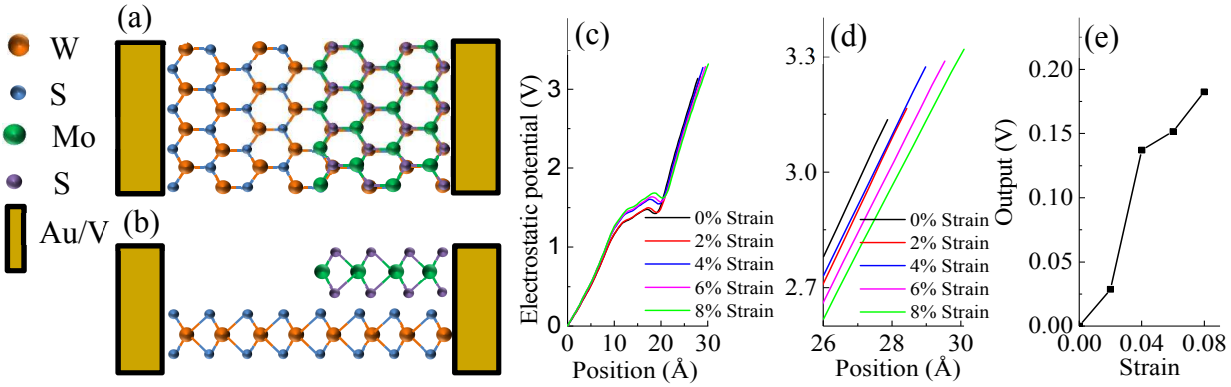

Figure 3. Schematic drawings of piezoelectric device with partial vertical heterostructure of WSe_2 and MoS_2 atomic layers in (a) top view and (b) side view. Electrostatic potential distribution between the electrodes for (c) whole heterostructure region and (d) near the right electrode. (e) Output voltage as a function of strain.

Figure 3 (a) and (b) show the piezoelectric device with partial vertical heterostructure of p-type WSe_2 and n-type MoS_2 atomic layers by AB stacking, where the chalcogenides (metals) in the top layer reside right above the metals (chalcogenides) in the bottom layer. The AB stacking with a short interlayer distance has a stronger vdW interaction than AA stacking[43]. Figure 3 (c) and (d) show the electrostatic potential distribution along the transport direction in the partial vertical heterostructure of WSe_2/MoS_2 for five different tensile strains with 2% increment of lattice parameter *a* along the transport direction. The larger (smaller) electrostatic potential is formed with the larger (smaller) depletion region. Figure 3 (e) shows the evolution of the output voltage as a function of the strain. The output voltages which are the electrostatic potential differences at right edge between the strained and the unstrained heterostructures are increased up to 0.137 eV and 0.183 eV for 4% and 8% strains, respectively.

Number of atomic layers

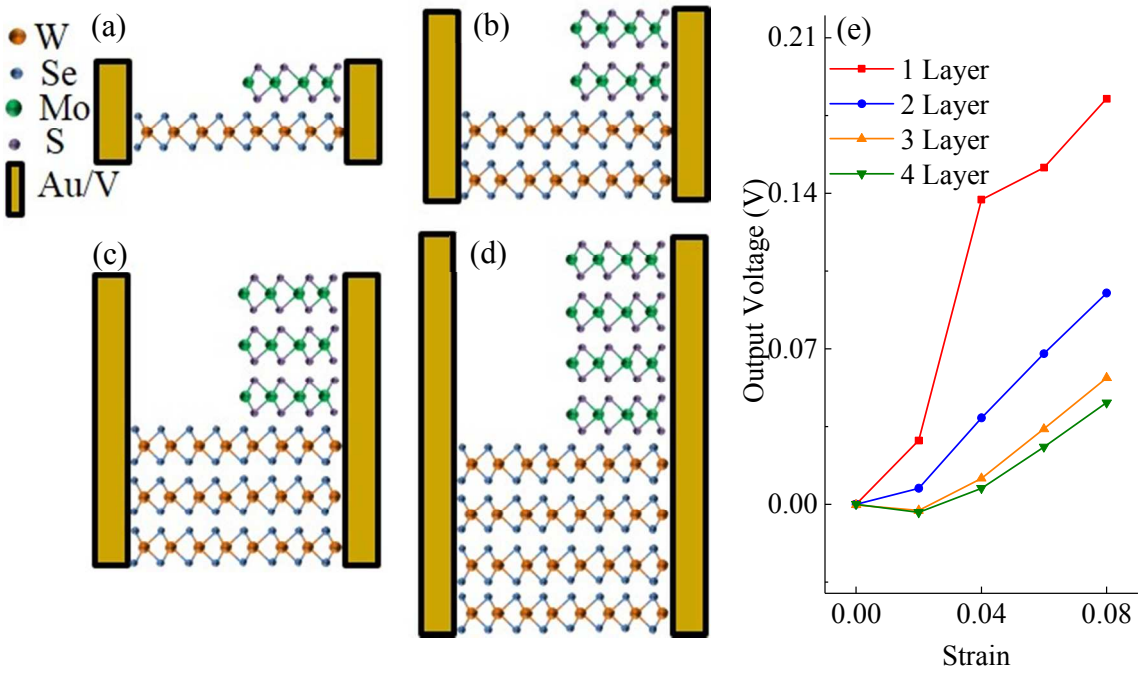

Figure 4. Schematic drawings of partial heterostructure piezoelectric devices with WSe_2/MoS_2 in AB-lattice stacking for different layers of (a) 1 layer, (b) 2 layers, (c) 3 layers, and (d) 4 layers. (e) Output voltage as a function of strain.

Figure 4 (a), (b), (c) and (d) display the schematic diagrams of partial heterostructure piezoelectric devices with WSe_2/MoS_2 in AB-lattice stacking for different layers of 1 layer, 2 layers, 3 layers, and 4 layers. The piezoelectric conversion output voltage as a function of stain is shown in figure 4 (e). The output voltage is monotonically decreased by increasing the number of layers. The output voltage was significantly decreased from 0.137 eV to 0.0072 eV for the heterostructure from 1 atomic layer to 4 atomic layers for 4% tensile strain. The smaller output voltage with the more number of atomic layers is due to the narrower band offset between WSe_2 and MoS_2, as shown in figure 1, where the electric polarization is attenuated in the heterostructure with multilayers.

Crystal stacking type

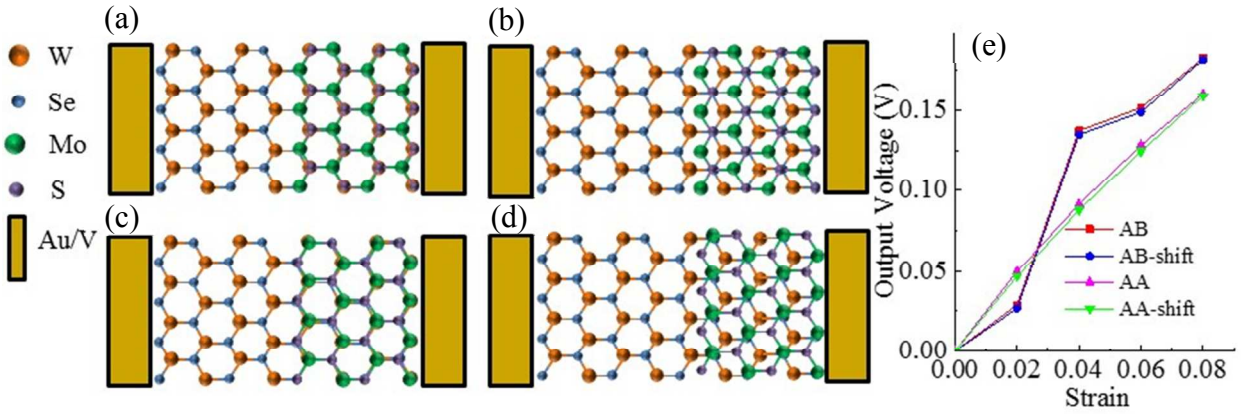

Figure 5. Schematic drawings of four different types of WSe_2/MoS_2 heterostructure piezoelectric devices with (a) AB-stacking, (b) AB-stacking shift, (c) AA-stacking, and (d) AA-stacking shift. (e) Output voltage as a function of strain for four different types of lattice stacking and layer shift.

The different lattice stacking in TMDCs has different interlayer interaction in heterostructure[44] which specifies the unique piezo-electronic property for each stacking type. Figure 5 (a), (b), (c), and (d) display the schematic drawings of four different types of WSe_2/MoS_2 heterostructure devices with AB-stacking, AB-stacking shift, AA-stacking, and AA-stacking shift. In the AB- and AA-stacking shift, the atomic layer is shifted to the opposite direction in parallel with the distance of a half lattice parameter. The figure 5 (e) shows the output voltage as a function of strain for the partial vertical heterostructure of WSe_2/MoS_2 with four different types of stacking. For the tensile strain larger than 4%, the heterostructures with AB-stacking and AB-stacking shift have the larger output voltage than those of the structures with AA-stacking and AA-stacking shift. The output voltage of heterostructure with AB-stacking was 0.137 V for 4% tensile strain, which is 50% higher than that of the heterostructure with AA-stacking. In comparison to AA-stacking, the AB-stacking heterostructure has the stronger interlayer coupling with the shorter interlayer distance, smaller band gap, and larger band offset[22]. Therefore, the AB-stacking heterostructure induces the larger piezoelectric response to the strain with the larger output voltage than that of AA-stacking. The output voltage difference between the stacking and the stacking shift is not visible.

Figure 6 shows the formation energy of partial and vertical heterostructures for four different stackings and stacking shifts. The formation energy is given by $E_{fm} = E_{WSe2/MoS2} - (E_{WSe2} + E_{MoS2})$, where $E_{WSe2/MoS2}$ is the total energy of heterostructure, E_{WSe2} and E_{MoS2} are the structural energies of WSe_2 and MoS_2 layers without layer interaction[45]. The total energy includes the exchange-correlation energy, kinetic energy, and electrostatic energy[46]. The lower formation energy

indicates better stability. The negative formation energies with AB-stacking and AB-stacking shift are due to the attraction between the oppositely charged ions of MoS_2 and WSe_2 at the interface of interlayer, while the positive formation energies with AA-stacking and AA-stacking shift are due to the repulsion between the ions with same charges of MoS_2 and WSe_2 at the interface of interlayer[47]. The lowest formation energy with AB-stacking indicates the best structural stability.

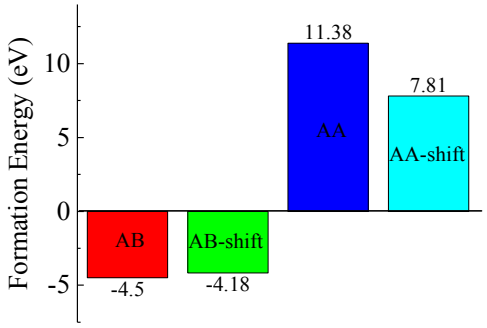

Figure 6. Formation energy of four different types of partial and vertical heterostructures with AB-stacking, AB-stacking shift, AA-stacking, and AA-stacking shift.

Interlayer interaction size

The schematic drawing of heterostructure piezoelectric devices of WSe_2/MoS_2 for the three different sizes of interlayer interaction are shown in figure 7 (a), (b), and (c). The length difference between two atomic layers is fixed to 3 unit cells. The three different sizes of interlayer interaction include 3, 4, and 5 unit cells. Figure 7 (d) shows the output voltage as a function of tensile strain for three different sizes of interlayer interaction. The heterostructure with the interlayer interaction size of 4 unit cells has the largest output voltage. The output voltages of heterostructure with the interlayer interaction size of three unit cells for 2% and 4% tensile strain are negative. It indicates that the left electrode acts as the anode, while the right electrode acts as the cathode. The reversal of the output polarity demonstrates that the band offset between WSe_2 and MoS_2 is reduced for the heterostructure with interlayer interaction area of 3 unit cells under 2% and 4% tensile strain. The separation distance between the layers also modifies the piezoelectric properties of heterostructure. The intrinsic interlayer distance between WSe_2 monolayer and MoS_2 monolayer was calculated to be 3.135 Å. The output voltages of heterostructure with interlayer distances of 4.0 Å and 7.0 Å were slightly modified from that with an interlayer distance 3.135 Å. It indicates that the interlayer distance change with a few

angstrom does not affect the piezoelectric conversion. However, the structural stability is significantly reduced by increasing the interlayer distance between WSe_2 and MoS_2.

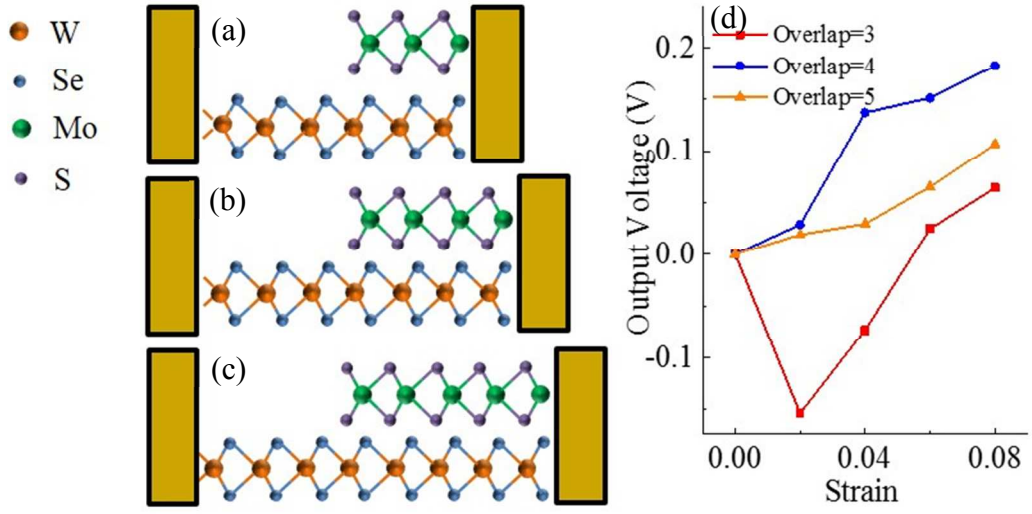

Figure 7. Schematic drawing of heterostructure of WSe_2/MoS_2 with three different interlayer interaction sizes of (a) 3, (b) 4, and (c) 5 unit cells. (d) Output voltage as a function of tensile strain for three different interlayer interaction sizes in unit cell dimension between WSe_2 and MoS_2.

II. Full vertical heterostructure

Figure 8 (a) shows the schematic drawing of piezoelectric device with a full vertical heterostructure of WSe_2/MoS_2. The heterostructure consists of *m* number of MoS_2 atomic layers and *n* number of WSe_2 atomic layers. The atomic layers in the heterostructure are stacked each other over the entire unit cells. Figure 8 (b), (c), and (d) display the electrostatic potential distribution along the transport direction (out-of-plane direction) of the heterostructure for 0%, 2%, 4%, 6% and 8% tensile strains. The electrostatic potential difference between the bottom edge and the top edge of unstrained (0%) heterostructure with MoS_2 monolayer and WSe_2 monolayer was 2.903 V. The electrostatic potential was increased as the tensile strain was increased. The electrostatic potential for 8% tensile strain was increased up to 3.1414 V between the bottom edge and the top edge of heterostructure. The change of electrostatic potential is due to the electronic or/and ionic polarization changes with atomic lattice deformation responding to the external stress.

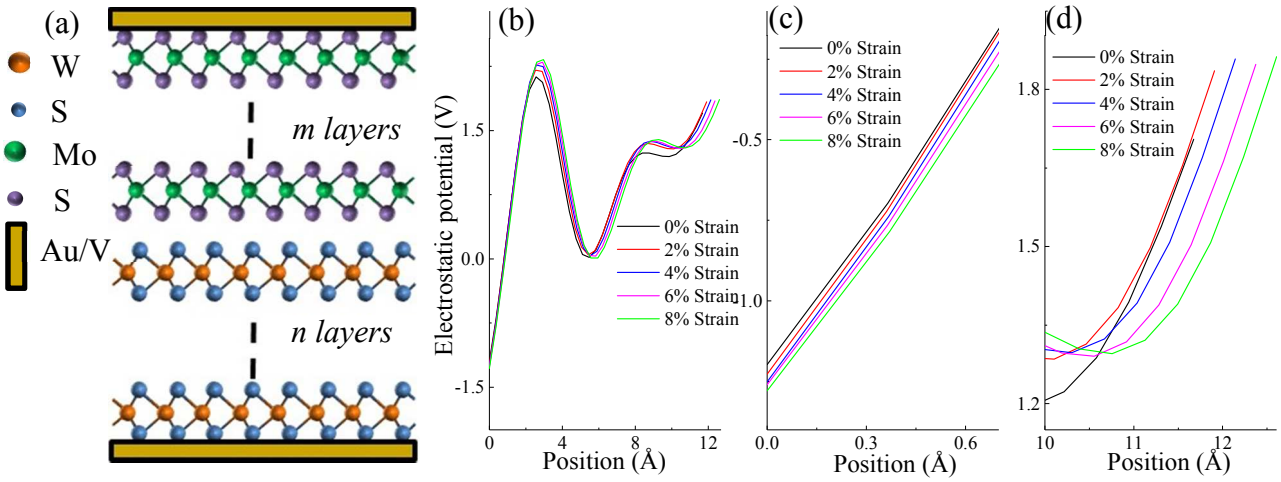

Figure 8. (a) Schematic drawing of full vertical heterostructure with *n* number of WSe_2 atomic layers and *m* number of MoS_2 atomic layers. Electrostatic potential distributions (b) along the entire transport distance, (c) at the left edge in the channel near the left electrode, and (d) at the right edge in the channel near the right electrode for the different tensile strains of 0%, 2%, 4%, 6% and 8%.

Figure 9 shows the output voltage as a function of tensile strain for the full vertical heterostructure with *m* number of MoS_2 atomic layers (*m*L) and *n* number of WSe_2 atomic layers (*n*L). The output voltage is monotonically increased as the tensile strain is increased. The output voltage is also dependent on the number of atomic layers in full vertical heterostructure. The output voltage of full vertical heterostructure with 1L-MoS_2 and 1L-WSe_2 is 0.239 V for the 8% tensile strain. However, the output voltage of heterostructure with 2L-MoS_2 and 2L-WSe_2 is 0.193 V for the 8% tensile strain. Compared to the output voltage with monolayer/monolayer heterostructure, the noticeable reduction of output voltage with bilayer/bilayer heterostructure is due to the reduction of band offset, as shown in figure 1 (a) and (b), and the attenuation of electric polarization by doubling the number of atomic layers. However, the output voltage (0.239 V) of full vertical heterostructure is higher than that (0.185 V) of partial vertical heterostructure under the same magnitude of tensile strain. It indicates that the larger interlayer coupling area of vertical heterostructure leads to the larger piezoelectric response.

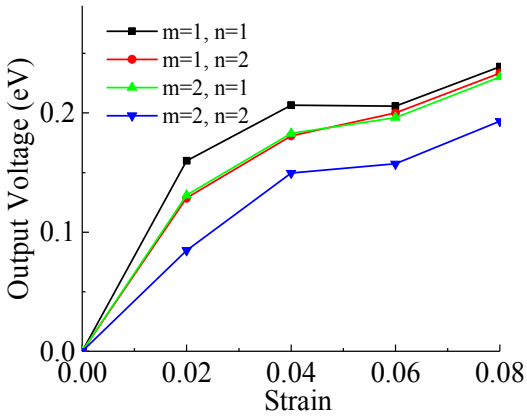

Figure 9. Output voltage as a function of tensile strain for the full vertical heterostructure with different number of layer combinations including 1L-MoS_2/1L-WSe_2, 1L-MoS_2/2L-WSe_2, 2L-MoS_2/1L-WSe_2, and 2L-MoS_2/2L-WSe_2.

Conclusion

The piezoelectronic properties of 2D WSe_2/MoS_2 heterostructure was investigated by first principle calculations with the density functional theory. The output voltage of partial vertical heterostructure atomic layers were 0.137 eV and 0.183 eV for 4% and 8% tensile strains, respectively. The different number of atomic layer, stacking type, and interlayer interaction size were the characteristic parameters of piezoelectricity for the partial and full vertical heterostructures. The output voltage of vdW heterostructure was significantly increased as the number of atomic layer was reduced. The large enhancement of output voltage was due to the large band offset and electric polarization with monolayer heterostructure. The output voltage of AB-stacking heterostructure of WSe_2/MoS_2 for the 4% tensile strain was larger than that of AA-stacking heterostructure for the same tensile strain due to the contribution of intrinsic piezoelectricity of each single layer in addition to the characteristic symmetric condition in out-of-plane. The interlayer interaction size modified the magnitude and polarity of output voltage. The intrinsic interlayer distance between 1L-MoS_2 and 1L-WSe_2 was 3.135 Å. The output voltage of full vertical heterostructure with 1L-MoS_2 and 1L-WSe_2 was 0.239 V for 8% tensile strain, while that of full vertical heterostructure with 2L-MoS_2 and 2L-WSe_2 was 0.193 V for the same strain. The large reduction of output voltage with bilayer/bilayer heterostructure was due to the reduction of band offset and the attenuation of electric polarization by doubling the number of atomic layers. The large output voltage of nanoscale partial or full vertical heterostructure was the unique piezoelectric property of 2D WSe_2/MoS_2 atomic layers with a large band offset.

Therefore, an additional enhancement of output voltage with a series connection of nanoscale piezoelectric devices will enable the realization of prospective NEMS with TMDC heterostructure atomic layers.

Acknowledgements

This work at HU is supported by ARO W911NF-15-1-0535, NSF HRD-1137747, and NASA NNX15AQ03A.

References

1 M. Z. Wang, in *2016 IEEE 16th International Conference on Nanotechnology (IEEE-NANO)*, 2016, pp. 875–878.
2 X. Q. Zheng, J. Lee and P. X. L. Feng, in *2015 Transducers - 2015 18th International Conference on Solid-State Sensors, Actuators and Microsystems (TRANSDUCERS)*, 2015, pp. 1393–1396.
3 S. Yu, K. Eshun, H. Zhu and Q. Li, *Sci. Rep.*, 2015, **5**, srep12854.
4 K. Kalantar-zadeh, J. Z. Ou, T. Daeneke, M. S. Strano, M. Pumera and S. L. Gras, *Adv. Funct. Mater.*, 2015, **25**, 5086–5099.
5 L. M. Malard, T. V. Alencar, A. P. M. Barboza, K. F. Mak and A. M. de Paula, *Phys. Rev. B*, 2013, **87**, 201401.
6 W. Wu, L. Wang, Y. Li, F. Zhang, L. Lin, S. Niu, D. Chenet, X. Zhang, Y. Hao, T. F. Heinz, J. Hone and Z. L. Wang, *Nature*, 2014, **514**, 470–474.
7 M. Noor-A-Alam, H. J. Kim and Y.-H. Shin, *Phys. Chem. Chem. Phys.*, 2014, **16**, 6575–6582.
8 K.-A. N. Duerloo, M. T. Ong and E. J. Reed, *J. Phys. Chem. Lett.*, 2012, **3**, 2871–2876.
9 S. Yu, Q. Rice, T. Neupane, B. Tabibi, Q. Li and F. J. Seo, *Phys. Chem. Chem. Phys.*, 2017, **19**, 24271–24275.
10 Y. Li, Y. Rao, K. F. Mak, Y. You, S. Wang, C. R. Dean and T. F. Heinz, *Nano Lett.*, 2013, **13**, 3329–3333.
11 X. Wang and F. Xia, *Nat. Mater.*, 2015, **14**, 264–265.
12 M. R. Neupane, in *2015 International Workshop on Computational Electronics (IWCE)*, 2015, pp. 1–2.
13 B. Zhu, X. Chen and X. Cui, *Sci. Rep.*, 2015, **5**, srep09218.
14 A. F. Rigosi, H. M. Hill, K. T. Rim, G. W. Flynn and T. F. Heinz, *Phys. Rev. B*, 2016, **94**, 075440.
15 H. Rostami, A. G. Moghaddam and R. Asgari, *Phys. Rev. B*, 2013, **88**, 085440.
16 A. M. Jones, H. Yu, N. J. Ghimire, S. Wu, G. Aivazian, J. S. Ross, B. Zhao, J. Yan, D. G. Mandrus, D. Xiao, W. Yao and X. Xu, *Nat. Nanotechnol.*, 2013, **8**, 634.
17 K. S. Novoselov, A. Mishchenko, A. Carvalho and A. H. C. Neto, *Science*, 2016, **353**, aac9439.
18 H. Fang, C. Battaglia, C. Carraro, S. Nemsak, B. Ozdol, J. S. Kang, H. A. Bechtel, S. B. Desai, F. Kronast, A. A. Unal, G. Conti, C. Conlon, G. K. Palsson, M. C. Martin, A. M. Minor, C. S. Fadley, E. Yablonovitch, R. Maboudian and A. Javey, *Proc. Natl. Acad. Sci. U. S. A.*, 2014, **111**, 6198–6202.
19 J. Kang, S. Tongay, J. Zhou, J. Li and J. Wu, *Appl. Phys. Lett.*, 2013, **102**, 012111.
20 N. R. Wilson, P. V. Nguyen, K. Seyler, P. Rivera, A. J. Marsden, Z. P. L. Laker, G. C. Constantinescu, V. Kandyba, A. Barinov, N. D. M. Hine, X. Xu and D. H. Cobden, *Sci. Adv.*, 2017, **3**, e1601832.
21 C. Zhang, C.-P. Chuu, X. Ren, M.-Y. Li, L.-J. Li, C. Jin, M.-Y. Chou and C.-K. Shih, *Sci. Adv.*, 2017, **3**, e1601459.
22 X. Hu, L. Kou and L. Sun, *Sci. Rep.*, 2016, **6**, srep31122.

23 M. Weismann and N. C. Panoiu, in *2016 IEEE 16th International Conference on Nanotechnology (IEEE-NANO)*, 2016, pp. 419–422.
24 H. Zhu, Y. Wang, J. Xiao, M. Liu, S. Xiong, Z. J. Wong, Z. Ye, Y. Ye, X. Yin and X. Zhang, *Nat. Nanotechnol.*, 2015, **10**, 151–155.
25 S. Manzeli, A. Allain, A. Ghadimi and A. Kis, *Nano Lett.*, 2015, **15**, 5330–5335.
26 X. Song, F. Hui, T. Knobloch, B. Wang, Z. Fan, T. Grasser, X. Jing, Y. Shi and M. Lanza, *Appl. Phys. Lett.*, 2017, **111**, 083107.
27 J. Qi, Y.-W. Lan, A. Z. Stieg, J.-H. Chen, Y.-L. Zhong, L.-J. Li, C.-D. Chen, Y. Zhang and K. L. Wang, *Nat. Commun.*, 2015, **6**, 7430.
28 S.-K Kim, R. Bhatia, T.-H. Kim, D. Seol, J.-H. Kim, H. Kim, W. Seung, Y. Kim, Y.-H. Lee, S.-W. Kim, *Nano Energy*, 2016, **22**, 483-489
29 X. Song, F. Hui, K. Gilmore, B. Wang, G. Jing, Z. Fan, E. Grustan-Gutierrez, Y. Shi, L. Lombardi, S. A. Hodge, A. C. Ferrari and M. Lanza, Nanoscale, 2017, 9, 6237–6245.
30 E. T. Yu, in III-V Nitride Semiconductors: Application and Devices, edited by E.T. Yu and O. Manaresh _Gordon and Breach, London, 2000.
31 A. Sarua, H. Ji, M. Kuball, M. J. Uren, T. Martin, K. J. Nash, K. P. Hilton and R. S. Balmer, Appl. Phys. Lett., 2006, 88, 103502.
32 L. Huang, Y. Li, Z. Wei and J. Li, *Sci. Rep.*, 2015, 5, 16448.
33 Y. Kobayashi, S. Yoshida, R. Sakurada, K. Takashima, T. Yamamoto, T. Saito, S. Konabe, T. Taniguchi, K. Watanabe, Y. Maniwa, O. Takeuchi, H. Shigekawa and Y. Miyata, Sci. Rep., 2016, 6, 31223.
34 M.-H. Chiu, C. Zhang, H.-W. Shiu, C.-P. Chuu, C.-H. Chen, C.-Y. S. Chang, C.-H. Chen, M.-Y. Chou, C.-K. Shih and L.-J. Li, *Nat. Commun.*, 2015, **6**, ncomms8666.
35 M. Brandbyge, J. L. Mozos, P. Ordejon, J. P. Taylor and K. Stokbro, *Phys. Rev. B Condens. Matter Mater. Phys.*, 2002, **65**, 165401.
36 W. Kohn and L. J. Sham, *Phys. Rev.*, 1965, **140**, A1133–A1138.
37 H. J. Monkhorst and J. D. Pack, *Phys. Rev. B*, 1976, **13**, 5188–5192.
38 J. P. Perdew, K. Burke and M. Ernzerhof, *Phys. Rev. Lett.*, 1996, **77**, 3865–3868.
39 R. O. Vianna, R. Custódio, H. Chacham and J. R. Mohallem, *Int. J. Quantum Chem.*, 1992, **44**, 311–318.
40 S. Grimme, *J. Chem. Phys.*, 2006, **124**, 034108.
41 A. Soba, E. A. Bea, G. Houzeaux, H. Calmet and J. M. Cela, *Comput. Phys. Commun.*, 2012, **183**, 2581–2588.
42 G. Makov and M. C. Payne, *Phys. Rev. B*, 1995, **51**, 4014–4022.
43 T. Peng, G. Huai-Hong, Y. Teng and Z. Zhi-Dong, *Chin. Phys. B*, 2014, **23**, 106801.
44 H. Heo, J. H. Sung, S. Cha, B.-G. Jang, J.-Y. Kim, G. Jin, D. Lee, J.-H. Ahn, M.-J. Lee, J. H. Shim, H. Choi and M.-H. Jo, *Nat. Commun.*, 2015, **6**, ncomms8372.
45 Z. Yang, Z. Lu, G. Luo and K. Hermansson, *Phys. Lett. A*, 2007, **369**, 132–139.
46 J. C. Slater and J. H. Wood, *Int. J. Quantum Chem.*, 1970, **5**, 3–34.
47 X. Hu, L. Kou and L. Sun, *Sci. Rep.*, 2016, **6**, 31122.